Applied Energy 160 (2015) 1–9

Contents lists available at ScienceDirect

Applied Energy

journal homepage: www.elsevier.com/locate/apenergy

Modeling on heat storage performance of compressed air in a packed bed system

Hao Peng, Rui Li, Xiang Ling *, Huihua Dong

Jiangsu Key Laboratory of Process Enhancement and New Energy Equipment Technology, School of Mechanical and Power Engineering, Nanjing Tech University, No. 30 Pu Zhu South Road, Nanjing 211816, PR China

HIGHLIGHTS

- The heat storage performance of compressed air in PBTES is presented.
- Effects of porosity, particle diameter and CA pressure on thermal behavior are investigated.
- The inlet CA pressure has significant influence on the thermal performance of PBTES.
- A packed bed filled with multiple HSMs has better charge efficiency.

ARTICLE INFO

Article history:
Received 1 February 2015
Received in revised form 7 July 2015
Accepted 6 September 2015
Available online 24 September 2015

Keywords:
Phase change material (PCM)
Compressed air
Packed bed
Thermal performance
Charge efficiency

ABSTRACT

Compressed Air Energy Storage (CAES) incorporates a Packed Bed Thermal Energy Storage (PBTES) represents a promising larger scale storage technology. The heat storage performance of compressed air (CA) in PBTES is presented and numerically analyzed in this paper. Phase change material (PCM) particles are used as the filler. The unsteady two-phase energy conservation equations considering the phase change phenomena inside the PCM particles are developed and solved numerically by finite difference method. This model has been validated with Izquierdo-Barrientos' experimental data. Then, the effects of porosity (ε), PCM particle diameter (d_p), CA inlet pressure (P) and filling approach on PBTES thermal behaviors (such as temperature profiles, heat storage capacity and charge efficiency) are investigated.

It was found that increasing particle diameter results in a decrease in the charge efficiency, and the charge efficiency increases with an increase in CA inlet pressure. The PBTES filled with three kinds of materials has better charge efficiency compared with the packed bed filled with single PCM or rock.

1. Introduction

As the energy crisis and environment pollution growing severely, the renewable energy sources is developed very fast for its inexhaustible, clean and environmentally friendly, especially of the solar and wind energy. However, they are intermittent by nature environment, which creates a demand for the energy storage system for the times when the source of energy is not available. The Compressed Air Energy Storage (CAES) is a promising and large-scale energy storage system which seems to be the good solution for the discontinuous problem of solar and wind energy [1–3].

For the traditional CAES system, the compressed air is released from the tank and heated up by additional energy sources like nature gas, fossil fuel, and then being expanded in a gas turbine. In order to avoid the use of additional energy, a new CAES system is developed. The heat generated during compression is stored and later released for heating up the compressed air before its expansion. A Packed Bed Thermal Energy Storage (PBTES) is adopted for this newly CAES system for its low cost, high efficiency and reliability.

Many researchers paid attention to the performance of PBTES system in recent years with different heat transfer fluids, such as molten salt [4–7], air [8,9], and water [10], not only for sensible PBTES, but also for latent PBTES. Ismail and Stuginsky [11] presented four kinds of models (Continuous solid phase model, Schumann's model, Single phase model and Thermal diffusion model) for simulating the thermal behavior of PBTES system. And the results of these models were compared and analyzed, both for sensible and latent.

Zanganeh et al. [12] designed a 7.2 GW h_{th} conical PBTES and the effects of the operational and design parameters on the performance of TES system were analyzed. Li et al. [13] studied the energy charge and discharge effectiveness of thermal storage

* Corresponding author. Tel.: +86 25 83587570; fax: +86 25 83600956.
E-mail address: xling@njtech.edu.cn (X. Ling).

http://dx.doi.org/10.1016/j.apenergy.2015.09.029
0306-2619/

Nomenclature

A	area of bed cross section (m^2)
A_w	wall effect correction term
B_w	wall effect correction term
D	diameter of storage tank (m)
E_{stored}	energy stored in the PCM particles (J)
E_{pump}	pumping energy (J)
E_{input}	input energy of molten salt (J)
Gr	Grashof number
H	storage tank height (m)
L_p	latent heat of PCM (kJ/kg)
M	maximum iterations for diameter of PCM sphere
N	maximum iterations for time step
Nu	Nusselt number
Pr	Prandtl number
ΔP	pressure drop (Pa)
R	Radius of storage tank
Re	Reynolds number
T	temperature (K)
T_{m1}	peak temperature of the PCM during the solid–solid transition (K)
T_{m2}	peak temperature of the PCM during the solid–liquid transition (K)
ΔT	temperature difference (K)
c_p	specific heat (J/kg K)
d_p	diameter of PCM spheres (m)
g	gravity (kg/m^2 s)
h	heat transfer coefficient (W/m^2 K)
h_a	volumetric heat transfer coefficient between air and solid (W/m^3 K)
h_l	overall heat loss coefficient
h_w	volumetric heat transfer coefficient between tank and ambience (W/m^3 K)
r	radius of PCM spheres (m)
t	time (s)
u	velocity (m/s)
x	location across the axis of the tank (m)

Greek symbols

ε	porosity
ρ	density (kg/m^3)
k	thermal conductivity (W/m K)
μ	dynamic viscosity (kg/m s)
ν	kinematic viscosity (m^2/s)
γ_{lh}	latent heat (J/kg)
η	charge efficiency
β	volumetric heat expansion coefficient of fluid (1/K)

Subscripts

a	air
ave	average
end	end
f	fluid
i	index for axial direction
in	inlet
out	outlet
l	liquid of PCM
L	low temperature
H	high temperature
m	index for radial direction
o	outer
p	particles
s	solid
surface	the surface of the tank

Superscripts

n	index for time step

tank. Zalba et al. [14] summarized the study of thermal energy storage, including materials, heat transfer and applications. Barton [15] presented simulation of thermal storage in a rock bed by considering the temperature-dependent density, and the effects of particle size, depth of bed and air flow rate were investigated. Bindra et al. [16] analyzed the recovered and lost exergy of PBTES system during cyclic storage and recovery. They found that the exergy efficiency of sensible heat storage system was higher than PCM storage system. Yang and Garimella [17] developed a model to study thermocline performance of the charge and discharge cycles of molten-salt in a PBTES system. Aldoss and Rahman [18] presented a new design for a PBTES system, and compared the thermal performance between the multi-PCM and single-PCM. Zanganeh et al. [19] designed a new TES filled with PCM and rocks. The simulations indicated that a PCM volume of 1.33% of the total storage volume was sufficient to achieve stabilization of the outflow air temperature when discharging. Anderson et al. [20] presented a packed bed filled with alumina and air was used as HTF, the thermal behavior of the PBTES was investigated both experimentally and numerically. Chai et al. [21] carried out an experimental study of a close loop PBTES system. It was found that the air flow direction has significant influence on the energy and exergy efficiencies. Chai et al. [22] also performed the experimental works on a cryogenic PBTES with liquid nitrogen as working fluid, and the influence of working pressure on the energy storage performance was analyzed.

Although there are many practical applications of PBTES system, however, very few works have been reported in literature on the topic of PBTES combined with a CAES system in general. Most recently, Liu et al. [23] published an important experimental study on the thermal performance of supercritical air blowing through a rock bed. The air pressure is ranged from 0.22 MPa to 6.55 MPa. As in their work, the air-to-solid heat transfer coefficients were measured and compared with various published correlations [24–28]. While the Yang's equations of non-uniform spherical particles were found to predict that coefficients very well. Also the effects of air pressure, mass flow rate and the entrance distances on the heat transfer coefficients were studied.

It is clear that Liu's work focuses on the heat transfer characteristics between the air and solid particles in packed bed system, however, the heat storage performances, such as heat storage capacity, charge efficiency were not performed. Besides, up to our knowledge, the thermal behavior of compressed air in PBTES has not been studied in the literature. Even though some well-developed models, as mentioned in Ref. [11], are capable of revealing the straight-forward phenomenon of CA in PBTES. It is also lack in a clear knowledge about the following two aspects so far: (1) the effects of some important factors, especially the CA pressure. Air is compressible fluid which is different from other heat transfer fluids, e.g., water or molten salts. The air properties variation with pressure is evident, that will affect the heat transfer performance in PBTES and need to be fully discussed; (2) various filling approaches. Most of previous works were considering the PBTES filling with single heat storage materials, the multiple filling approaches have not been evaluated.

Accordingly, it is the goal of the present work to present a numerical model of CA in PBTES system. As indicated by Ref. [23], Yang's correlations are adopted to calculate the air-to-solid

heat transfer coefficient. The charge efficiency and the heat transfer phenomena during charge of the PCM are investigated. Also the effects of porosity, PCM particle diameter, CA inlet pressure and filling approach on PBTES thermal behaviors are presented. Based on these numerical studies, guidelines are provided for designing and optimizing PBTES in a CAES system with various operating conditions.

2. PBTES description

A brief schematic diagram of CAES system using packed bed is presented in Fig. 1. The cycle of the system is summarized below. During the charge time, air from environment is compressed by compressor, which is driven by solar or wind energy. Compression air heat energy is stored in PBTES for future use. The process of compression and heat storage will be repeatedly before CA comes into the air storage. During the discharge time, the high pressure CA in storage tank and the heat stored in PBTES are released. The CA firstly heated by the PBTES and enters turbine and outputs work subsequently. In the present study, the PBTES bed is assumed to be a vertical cylinder which has entrance on the top and exit on the bottom, and it can be filled with single heat storage material (HSM) or multiple HSMs.

The height (H) and diameter (D) of packed bed are 2 m and 1 m, respectively. The PCM ($NaNO_2$) is filled at a porosity (ε) of 0.4. Table 1 shows the basic parameters characteristics of the PBTES. The main properties of the PCM are measured by Differential Scanning Calorimeter NETZSCH DCS F3 (−40 °C to 600 °C) and NETZSCH LFA457 MicroFlash (−125 °C to 1100 °C) in our lab, which are shown in Table 2. The properties of CA changing with temperature and pressure can be looked up in Ref. [29].

Table 1
Operational parameters of packed bed.

Parameters	Values
Height of packed bed (H)	2 m
Diameter of packed bed (D)	1 m
Tank insulation material	Expanded perlite
Thickness of insulation	100 mm
Porosity (ε)	0.4
Heat transfer fluid (HTF)	Compressed air
The flow velocity of HTF	0.5 m/s
Phase change material (PCM)	$NaNO_2$
Diameter of PCM capsule (d_p)	20 mm
CA inlet pressure (P)	2.0 MPa
Operating temperature (T)	450–600 K

Table 2
Thermo-physical properties of PCM.

Parameters	$NaNO_2$
Melting temperature (K)	550.47–576.80
Density (solid) (kg/m^3)	2097 (at 538.15 K)
Density (liquid) (kg/m^3)	1873 (at 600 K)
Specific heat (solid) (J/kg K)	1385 (at 538.15 K)
Specific heat (liquid) (J/kg K)	1514 (at 600 K)
Thermal conductivity (solid) (W/m K)	0.562 (at 538.15 K)
Thermal conductivity (liquid) (W/m K)	0.476 (at 600 K)
Dynamic viscosity (liquid) (kg/m s)	2.54×10^{-3} (at 600 K)
Latent heat (kJ/kg)	199.6

3. Mathematic model of PBTES

3.1. Modeling heat transfer in PBTES

Fluid and solid heat transfer in the PBTES is complicated and the energy transport combines convection and conduction. To simplify the model, there are some assumptions as follows:

(1) The properties of CA are homogeneous and calculated at an average temperature $T_{ave} = (T_{in} + T_{out})/2$.
(2) Variation of temperature along the radial direction is neglected.
(3) Uniform distribution porosity is applied to the packed bed.
(4) Ignore the volume change of fluid and solid particle caused by the temperature change.
(5) Internal heat generation is not considered in packed bed.
(6) Radiation is negligible.

Based on the above assumptions, an unsteady continuous solid phase model is used to analyze the heat transfer within the packed bed. The energy conservation equations are:

For the fluid phase:

$$\varepsilon\rho_a c_{pa}\left(\frac{\partial T_a}{\partial t} + u_a\frac{\partial T_a}{\partial x}\right) = \varepsilon k_a\frac{\partial^2 T_a}{\partial x^2} + \frac{6(1-\varepsilon)h}{d_p}(T_s - T_a) + h_w(T_w - T_a) \quad (1)$$

For the solid phase:

$$(1-\varepsilon)\rho_s c_{ps}\frac{\partial T_s}{\partial t} = (1-\varepsilon)k_s\frac{\partial^2 T_s}{\partial x^2} + \frac{6(1-\varepsilon)h}{d_p}(T_a - T_s) \quad (2)$$

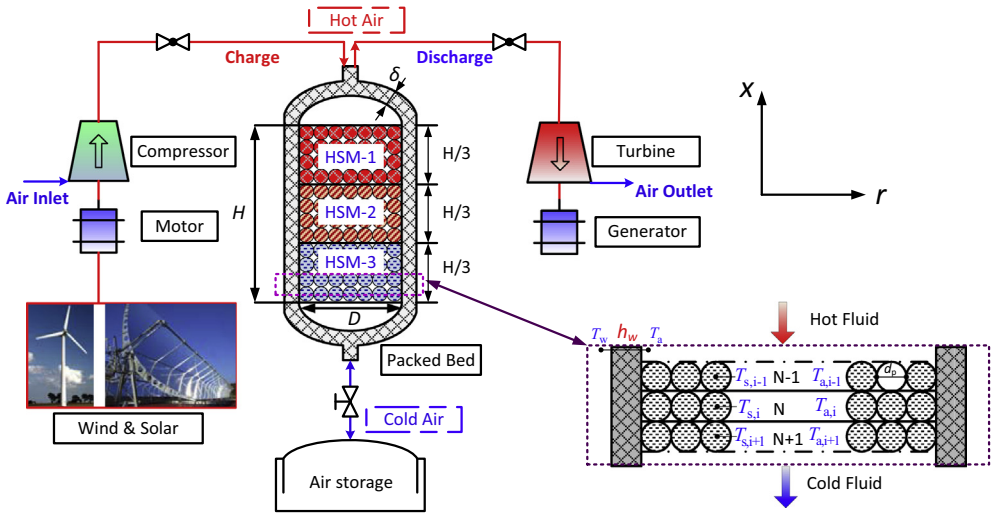

Fig. 1. Schematic of packed bed thermal storage system.

The heat transfer coefficient h between CA and solid is calculated using Yang et al. [28]

$$Nu = \frac{hd_p}{k_a} = 2.2 + 0.56Pr^{1/3}Re_p^{0.65} \tag{3}$$

where

$$Pr = \frac{c_{pa}\mu_a}{k_a}; \quad Re_p = \frac{\rho_a d_p \varepsilon u_a}{\mu_a}$$

The volumetric heat transfer coefficient between vessel and ambient is given by:

$$h_w = h_l \frac{2\pi R_o}{\pi R_i^2} = h_l \frac{2R_o}{R_i^2} \tag{4}$$

The overall heat loss coefficient h_l through the wall is given by Ref. [20]

$$\frac{1}{h_l} = \frac{D_i \ln\frac{D_o}{D_i}}{2k_{\text{insulation}}} + \frac{1}{h_{\text{wall}}} \tag{5}$$

$$Nu(x) = \left[\frac{7Gr(x)Pr^2}{100 + 105Pr}\right]^{1/4} + \frac{4(272 + 315Pr)}{35(64 + 63Pr)}\frac{x}{D_o} = \frac{h_{\text{wall}}x}{k_a} \tag{6}$$

$$Gr(x) = \frac{\beta g(T_{\text{surface}} - T_w)x^3}{v^2} = \frac{g(T_{\text{surface}} - T_w)x^3}{v^2(T_{\text{surface}} + T_w)} \tag{7}$$

For PCM particle internal temperature distribution:

$$\rho_p c_{p,p}\frac{\partial T_p}{\partial t} = k_p\left[\frac{\partial^2 T_p}{\partial r^2} + \frac{2}{r}\frac{\partial T_p}{\partial r}\right] \tag{8}$$

This energy equation is applicable to the sensible HSM. However, for modeling the phase change process inside PCM particles, enthalpy method was used. This method regards the phase change process occurring in a small temperature range and takes the latent heat as a large heat capacity in the temperature range.

It can be achieved by considering the temperature dependent thermo-physical properties to meet the needs of the phase change process inside PCM, which the effective specific heat ($c_{p,p}$) and thermal conductivity (k_p) are expressed as:

$$c_{p,p} = \begin{cases} c_{p,ps}, & T_p < T_{m1} \quad \text{solid} \\ \frac{c_{p,ps}+c_{p,pl}}{2} + \frac{\gamma_{lh}}{\Delta T_{lh}}, & T_{m1} < T_p < T_{m2} \quad \text{solid—liquid transition} \\ c_{p,pl}, & T_p > T_{m2} \quad \text{liquid} \end{cases} \tag{9}$$

$$k_p = \begin{cases} k_{p,s}, & T_p < T_{m1} \quad \text{solid} \\ \frac{k_{p,s}+k_{p,l}}{2}, & T_{m1} < T_p < T_{m2} \quad \text{solid—liquid transition} \\ k_{p,l}, & T_p > T_{m2} \quad \text{liquid} \end{cases} \tag{10}$$

3.2. Charge efficiency calculation

The charge efficiency is the key performance indicator of thermal storage in the packed bed during the charge process. In the present study, considering heat loss through the wall and the pump work, the charge efficient is defined as:

$$\eta_{\text{charge}} = \frac{E_{\text{stored}}}{E_{\text{input}} + E_{\text{pump}}} \tag{11}$$

E_{stored} is the energy stored in solid heat storage materials:

$$E_{\text{stored}} = \int_0^H A[(1-\varepsilon)\rho_s c_{ps}(T_s(x) - T_0) + \varepsilon\rho_a c_{pa}(T_a(x) - T_0)]dx \tag{12}$$

E_{input} is the releasing energy of CA entering and exiting the storage tank, which is given by:

$$E_{\text{input}} = \int_0^{t_{\text{end}}}\int_{T_{\text{out}}}^{T_{\text{in}}} A\varepsilon u_a \rho_a c_{pa} dTdt \tag{13}$$

E_{pump} is the pump work and can be defined as:

$$E_{\text{pump}} = \int_0^{t_{\text{end}}} A\varepsilon u_a \Delta P dt \tag{14}$$

where Δp is the pressure drop across the packed bed and can be calculated by Ergun equations [30].

$$\frac{\Delta P}{\rho_a(\varepsilon u_a)^2}\frac{d_p}{H} = \frac{K_1 A_w}{Re}\frac{(1-\varepsilon)^2}{\varepsilon^3} + \frac{A_w}{B_w}\frac{(1-\varepsilon)}{\varepsilon^3} \tag{15}$$

$$A_w = 1 + \frac{2}{3(D/d_p)(1-\varepsilon)}$$

$$B_w = \left[k_1\left(\frac{d_p}{D}\right)^2 + k_2\right]^2$$

where K_1 is coefficient of pressure drop correlation, k_1 and k_2 are coefficient of wall effect correction terms. In the presented work, K_1 = 154, k_1 = 1.15, k_2 = 0.87, respectively.

3.3. Simulation procedure

3.3.1. Initial and boundary conditions

The initial and boundary conditions for charge process

$$T_a(t=0) = T_0; \quad T_s(t=0) = T_0 \tag{16}$$

The boundary conditions for PCM particles

$$r = \frac{d_p}{2}, \quad T_p = T_s \tag{17}$$

$$r = 0, \quad \frac{\partial T_p}{\partial r} = 0 \tag{18}$$

3.3.2. Computational method

Finite different method is used to solve the mathematic model developed in Section 3. Fig. 2 illustrates the schematic of solution procedures. The PBTES is divided into N elements along the axis direction. Let Δx denote the element step size. $T_{a,i}^n$ and $T_{s,i}^n$ are calculated for temperature of CA and solid particles at time step n and the element i. $T_{p,m}^n$ is temperature distribution inside the solid particles, The black frame is the definition of variables for cell n.

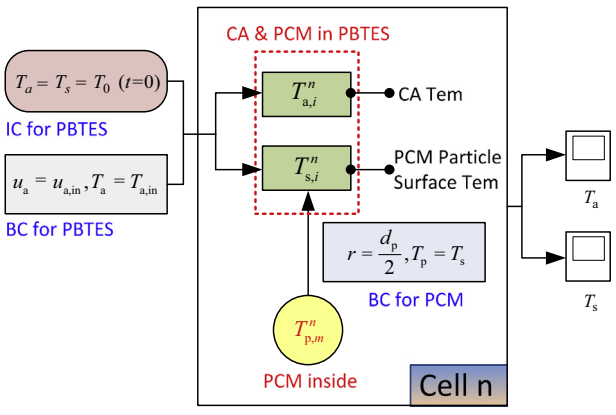

Fig. 2. Schematic of solution procedures.

The detailed solution procedures are described as follows:

(1) Set the initial conditions (IC) and boundary conditions (BC) for PBTES.
(2) Calculate the heat transfer in PCM particles, Eq. (8) is interpreted as:

$$\rho_p c_{p,p}\frac{T_{p,m}^{n+1}-T_{p,m}^{n}}{\Delta t}=k_p\left[\frac{T_{p,m+1}^{n+1}-2T_{p,m}^{n+1}+T_{p,m-1}^{n+1}}{\Delta r^2}+\frac{2}{r}\frac{T_{p,m}^{n+1}-T_{p,m-1}^{n+1}}{\Delta r}\right] \tag{19}$$

Based on the boundary conditions for PCM particles, $T_{p,m}^{n+1}$ and the mean value $\overline{T}_{p,i}^{n+1}$ ($\overline{T}_{p,i}^{n+1}=\sum_{i=1}^{M}T_{p,m}^{n+1}/M$) can be calculated.
(3) Set the related PCM properties ($c_{p,p}$ and k_p) corresponds to the mean temperature $\overline{T}_{p,i}^{n+1}$.
(4) Finite different method applied to the energy equations (1) and (2) for each cell, and can be dispersed as:

$$\begin{aligned}&\varepsilon\rho_a c_{pa}\left(\frac{T_{a,i}^{n+1}-T_{a,i}^{n}}{\Delta t}+u_a\frac{T_{a,i}^{n+1}-T_{a,i-1}^{n+1}}{\Delta x}\right)\\&\quad=\varepsilon k_a\frac{T_{a,i+1}^{n+1}-2T_{a,i}^{n+1}+T_{a,i-1}^{n+1}}{\Delta x^2}+\frac{6(1-\varepsilon)h}{d_p}(T_{s,i}^{n+1}-T_{a,i}^{n+1})\\&\qquad+h_w(T_w-T_{a,i}^{n+1})\end{aligned} \tag{20}$$

$$\begin{aligned}(1-\varepsilon)\rho_s c_{ps}\frac{T_{s,i}^{n+1}-T_{s,i}^{n}}{\Delta t}&=(1-\varepsilon)k_s\frac{T_{s,i+1}^{n+1}-2T_{s,i}^{n+1}+T_{s,i-1}^{n+1}}{\Delta x^2}\\&\quad+\frac{6(1-\varepsilon)h}{d_p}(T_{a,i}^{n+1}-T_{s,i}^{n+1})\end{aligned} \tag{21}$$

Firstly, use $\overline{T}_{p,i}^{n+1}$ instead of $T_{s,i}^{n+1}$ on the left-hand side of Eq. (21). Then, Jacobi iteration method is adopted to solve the tri-diagonal matrix Eqs. (20) and (21) and the unknown values $T_{a,i}^{n+1}$ and $T_{s,i}^{n+1}$ can be calculated and updated by iterations.

(5) Repeat the iterations until the number of step reached N.
(6) Repeat the loop until the time step reached t_{end}.

4. Grid independence and model validation

4.1. Grid independence

The grid independence was done on the PBTES system for a case of d_p = 25 mm, ε = 0.4 and P = 2.0 MPa. Five different sets of cell number (400–5000) were employed to show the influence of grid density on the numerical results. The compressed air temperature (T_a) and PCM temperature (T_s) at the center of storage tank (H = 1 m) were listed and showed in Table 3 and Fig. 3. The relative error of the T_a and T_s between the grid of 4000 and 5000 are less than 0.1%. In order to save computational resource and keep an adequately accuracy, the cell number about 4000 was adopted for the results presented below, as shown in Fig. 3.

4.2. Model validation

This section contains a validation of the numerical method according to an example performed by Izquierdo-Barrientos et al.

Table 3
T_a and T_s of different grid numbers.

Grid number	400	1000	2000	4000	5000
T_a (K)	493.17	483.55	479.49	477.77	477.35
T_s (K)	488.95	479.19	475.44	473.46	473.05

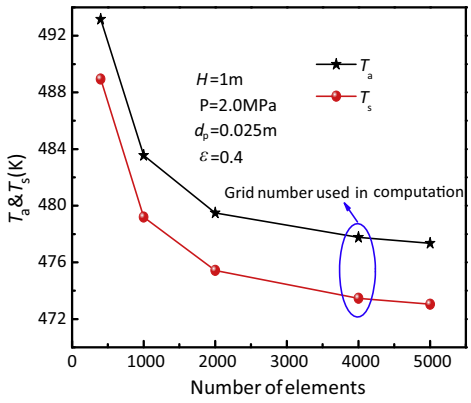

Fig. 3. Grid independence.

Table 4
Data for the validation (from Izquierdo-Barrientos et al. [31]).

Parameters	Units	Value
PCM	/	Coarser-GR50
Heat transfer fluid	/	Air
Porosity of PCM	/	0.486
Height of the bed (H)	mm	200
Diameter of the bed (D)	mm	200
Particle diameter (d_p)	mm	1.64
Specific heat of PCM in solid phase (c_{ps})	J/kg K	1448.6
Specific heat of PCM in liquid phase (c_{pl})	J/kg K	1735.7
Density of PCM (ρ_s)	kg/m^3	1512.8
Thermal conductivity of PCM (k_s)	W/m K	0.2
The flow rate of air	l/min	450

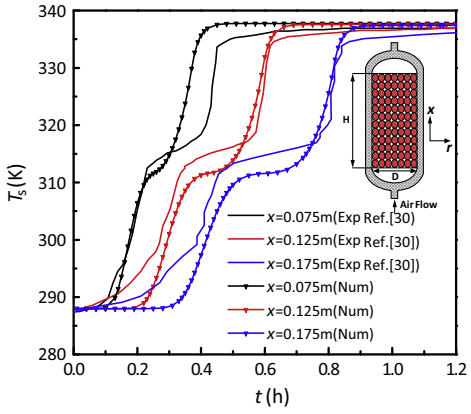

Fig. 4. Comparison between the present numerical simulation and experimental data in Ref. [31].

[31]. The basic data for validation is shown in Table 4. The comparison between numerical results and experimental data are shown in Fig. 4 for the height x = 0.075 m, x = 0.125 m, and x = 0.175 m. In Fig. 4, the results of the validation test appear identical, the average deviations of T_s are less than 7% for x = 0.075 m and 5% for x = 0.125 m, respectively. For the numerical simulation, the phase change takes place at different heights at different time because of the temperature stratification, in accordance with results presented by the experiments.

As can be seen, although both tendencies of the present simulation results and experimental data agree well, their values vary obviously, especially for the time range from 0.3 h to 0.5 h. This deviation is dominated by the heat transfer coefficient h between the solid PCM and air, if the correlation of h is reasonable, the

similarity in the results is not surprising. In the present work, Eq. (2) shows the empirical definition of h, which is given by [28], it depends on the air flow velocity and the air properties. As the operating conditions (air flow velocity and properties) and geometrical parameters are absolutely the same with the Ref. [23], the simulation results are acceptable because of the less average deviations mentioned above. However, other correlations for calculating h, for instance the model developed by Wakao and Kagei [27], which was unable to model the experimental results well (not shown).

Therefore, it can be concluded that the presented numerical model, especially the correlations of h, is reasonable for the performance prediction of the PBTES. Thereinafter the effects of porosity, PCM particle diameter, air inlet pressure and filling approach are investigated by the corresponding numerical method.

5. Results and analysis

5.1. Temperature profiles of compressed air (CA) and PCM

The temperature distributions of the CA and PCM particles and at three different positions (x = 0.5, 1.0, 1.5 m) on the center line of the model are shown in Fig. 5. The initial temperature of the packed bed is set to be 450 K and the CA pressure is 2.0 MPa. The changing trends of three curves are similar. Because the energy stored in CA is transferred to the solid particles during charge process, the CA temperature is higher than PCM temperature.

In Fig. 5, the charge process can be divided into three regions. The first region is characterized by sensible heat transfer, which the PCM temperature increases rapidly. Interestingly, there is a downtrend of PCM temperature at the initial time as due to the heat loss through the wall. The followed region is that the value of PCM temperature reaches to the phase transition period ($T_{m1} < T_s < T_{m2}$, denoted by the dash line in Fig. 5). In this region, the temperature gradient approximately has a flat slope for the increase of charge time, which is caused by the latent heat storage in PCM particles. At the end of phase change (final region), the temperature increases fast until the charge process is terminated.

5.2. Effect of porosity

Generally, a lower porosity benefits a cost-effective PBTES system, however, the effect of porosity need to be studied. Fig. 6 shows the temperature distributions of CA and PCM particles for different porosity varied in the range between 0.3 and 0.5 at t = 1.5 h. The temperatures of CA and PCM increase with an increase in porosity at the same position. This is due to the fact that

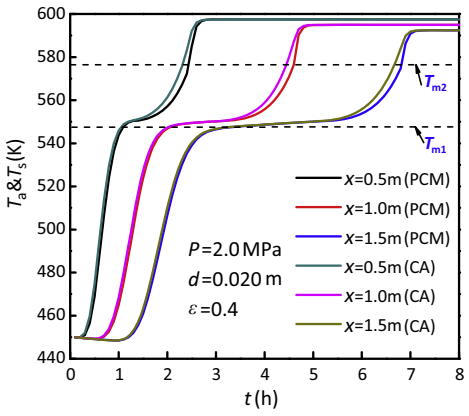

Fig. 5. Temperature profiles of CA and PCM particles across the PBTES versus storage time.

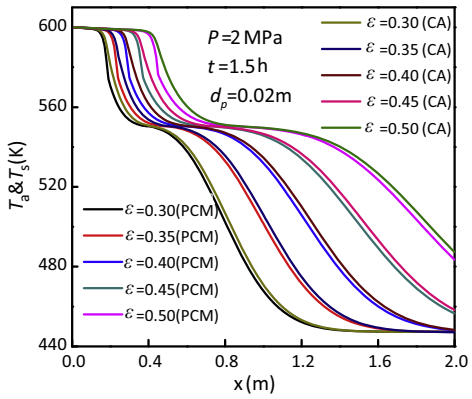

Fig. 6. Temperature profiles of CA and PCM particles at t = 1.5 h versus the axial height for different porosity.

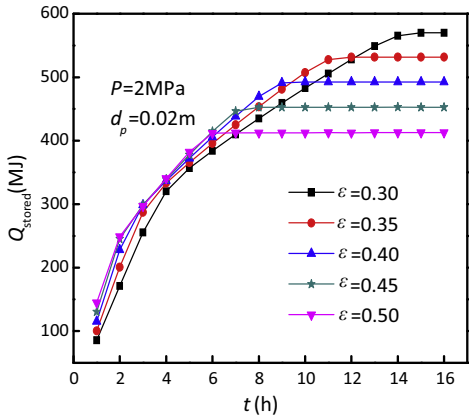

Fig. 7. Heat storage capacities versus charge time for different porosity.

more space is occupied by CA for a larger porosity, the capacity of heat storage reduces relatively, and the heat transferred from CA to PCM also weakens.

The comparison of heat storage capacity with different porosity during charge process is shown in Fig. 7. The thermal storage capacity rises approximately in a straight line at the beginning and it goes up at a slight lower speed during melting until reaching the maximum capacity. These upward trends for different porosity are similar. Higher porosity leads to markedly lower thermal storage capacity but it takes less time to complete heat storage. Take two curves (ε = 0.3 and ε = 0.5) for instance, with the increase in porosity from 0.3 to 0.5, the maximum capacity is decreases from 560 MJ to 410 MJ, accordingly, the charge time is also decreases from approximately 14 h to 6 h.

Fig. 8 shows the charge efficiency of PBTES system for different porosity. As can be seen, at the initial charge period, the larger the porosity is, the higher the efficiency is. This is because a larger porosity means that the packed bed was filled with more high temperature CA and the heat transfer rate also can be enhanced by a larger temperature difference between CA and PCM, which results in a higher efficiency at first. As time goes on, the charge efficiency decreases with an increase in storage time, and higher porosity corresponds to a faster decline rate so that leads to lower charge efficiency. This is due to the temperature difference between storage tank wall and the ambient plays an important role in calculation of charge efficiency. At the beginning of charge process, the temperature different is not significantly big, so the heat loss to the surrounding is small resulting in a slightly difference of the charge efficiency. However, with the increase of time, since

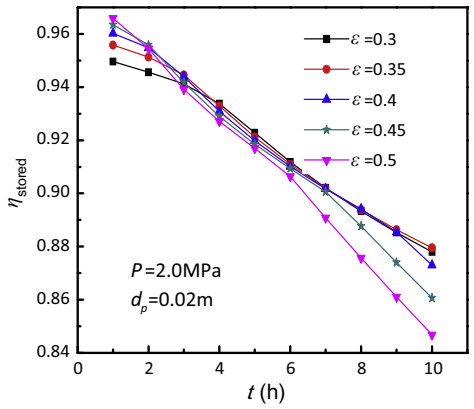

Fig. 8. Charge efficiency versus charge time for different porosity.

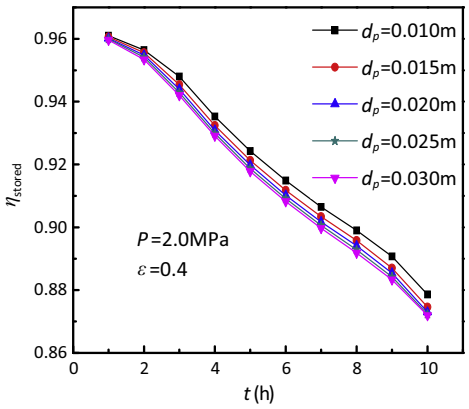

Fig. 10. Charge efficiency versus charge time for different particle diameter.

the larger porosity allows a faster temperature rise indicated by a higher heat loss. As a result, the charge efficiency for $\varepsilon = 0.5$ is lower at the end.

5.3. Effect of PCM particle diameter

Fig. 9 presents PCM temperature distributions across the storage height for d_p = 0.010, 0.015, 0.020, 0.025, 0.030 m at t = 1.5 h. The porosity and the inlet CA pressure are 0.4, 2 MPa, respectively. It can be seen from the plot, with the decrease in particle diameter, the PCM temperature decreases with a higher rate in the front position. Extraordinary, there is a turning point for the PCM temperature around x = 0.6. This is because the heat transfer coefficient between CA and PCM particles is increased with the decrease of particle diameter, which results in a thinner temperature gradient region. With the decrease in PCM diameter from 0.03 m to 0.01 m, the thickness of temperature gradient decreases from about 1.59 m to 1.21 m.

Accordingly, the charge efficiencies of five different particle diameters decrease over time (Fig. 10). Smaller diameter leads to higher charge efficiency. This is due to the heat transfer process between CA and PCM particle surface and within the PCM particle depends highly on the particle size, which can be demonstrated by the trends of representative CA temperature distribution as plotted above in Fig. 9. Actually, there is less obvious distinction among these curves, indicating that the PCM particle diameter has a little influence on charge efficiency in fact.

Also there is no significant different in heat storage capacity for different particle diameters, as shown in Fig. 11. At the initial stage

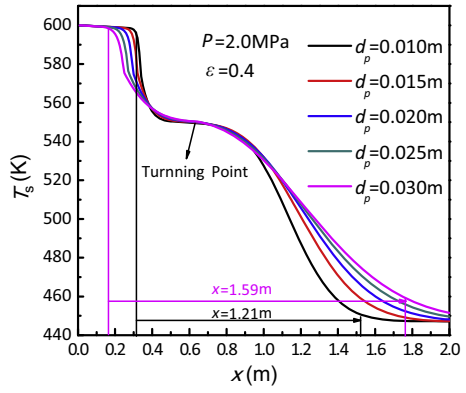

Fig. 9. Temperature profiles of PCM particles versus the axial height for different particle diameter.

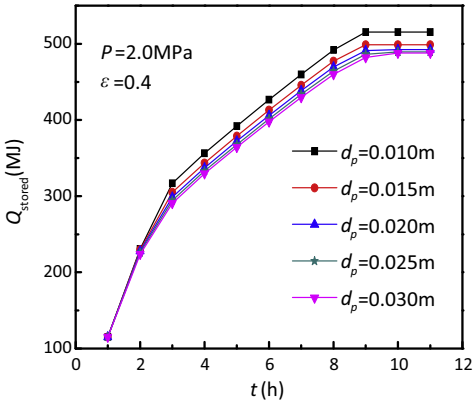

Fig. 11. Heat storage capacities versus charge time for different particle diameter.

of charge process the capacity increases with an increase of charge time. During melting process, the rising trends of the capacity become slow. The heat storage capacity reaches the maximum in the final stretch of charge process. As different particle diameter causes the change of CA Reynolds number, there exists in different local thermal non-equilibrium and temperature difference which leads to a slight difference of the maximum heat storage capacity.

5.4. Effect of inlet CA pressure

Fig. 12 shows the temperature profiles of CA and PCM particles for different CA inlet pressure varying from 0.5 MPa to 2.5 MPa at t = 1.5 h. The particle diameter and the porosity remain constant over the charge time and are 0.020 m, 0.4, respectively. It can be seen that the temperatures of CA and PCM increase with an increase in inlet CA pressure, as well as the temperature gradient region.

Heat storage capacities for different CA pressures are shown in Fig. 13. The heat storage capacity rises in a straight line and higher CA pressure leads to larger rate of capacity rise. However, there is discrepancy among five curves in the final stage. The total storage time is extended significantly with the decreases of the CA pressure. For instance, with the decrease in CA pressure from 2.5 MPa to 2.0 MPa, the time needed for total heat storage capacity reaches 500 MJ expands from 7.1 h to 9 h. This is due to the fact that the physical properties of CA vary under different pressures and the CA in higher pressure is much easier to be distributed in PBTES so that there is less different of CA temperature along the axis, which agrees well with the expanded temperature gradient region as illustrated in Fig. 12. Therefore, it can be deduced from this

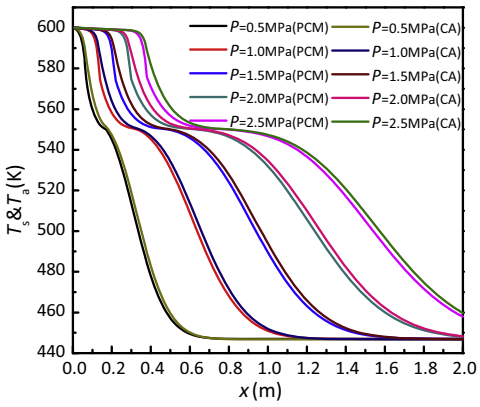

Fig. 12. Temperature profiles of CA and PCM particles versus the axial height for different inlet CA pressure at t = 1.5 h.

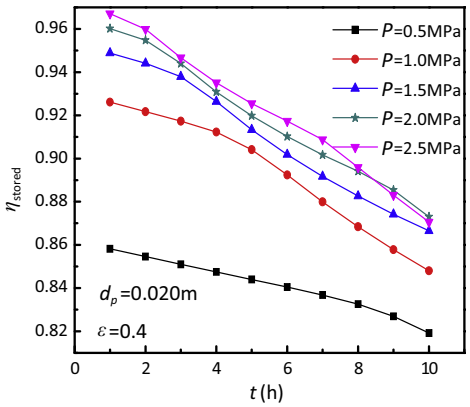

Fig. 14. Charge efficiency versus charge time for different inlet CA pressure.

figure that, although the rate of capacity is different, the total heat storage capacities are almost the same.

Fig. 14 presents the changes of charge efficiency for different CA pressures. It is clear that with the increase of inlet pressure, the charge efficiency is higher. These higher charge efficiencies primarily result from the enhanced heat transfer between CA and PCM particles with higher CA pressure. Therefore, it can be concluded from Figs. 12–14 that, the inlet CA pressure has significant influence on the thermal performance of PBTES. Increasing the inlet CA pressure can contribute to faster temperature expansion and thus a thicker temperature gradient region. And that finally brings about shortened charge time and increased charge efficiency. On the other hand, it should also be noted here that inlet CA pressure of 0.5 MPa and 1.0 MPa lead to considerable difference as shown in Fig. 14, which means that the influence of CA pressure on the thermal behavior becomes evident when the CA pressure is small. Therefore, to achieve high system performance and charge efficiency, the PBTES should operate at a higher inlet CA pressure, e.g., higher than about 1.0 MPa.

5.5. Effect of filling approach

Fig. 15 shows temperature profiles of PCM particles versus charge time for single PCM, rock and multiple HSMs at x = 1.5 m. For multiple HSMs, rock, steel and PCM ($NaNO_2$) are filled as HSM-1, HSM-2 and HSM-3 as shown in Fig. 1. The specific heat, density and thermal conductivity of rock are 960 J/(kg K), 2560 kg/m^3, 0.48 W/(m K), respectively. And the specific heat, density and thermal conductivity of steel are 571 J/(kg K), 7800 kg/m^3, 50 W/(m K), respectively [8]. For comparison study, the PBTES of three different filling approaches are simulated with the same initial and operating conditions.

As shown in Fig. 15, during the early period of charge process, the temperature of single PCM rises faster than that of others. As time goes on, the PCM begins to melt so that the temperatures of PCM particles have a slower upward trend and temperature of PBTES filled with rock is higher than that of others. Simultaneously, the temperature profile of multiple HSMs shows a degressive slop around t = 3 h due to the melting process of PCM. Because the PCM was filled near the exit of the PBTES, it started to melt a little later but melted faster than single PCM.

Fig. 16 shows the comparison of charge efficiency for different filling approaches. Firstly, the charge efficiency of PBTES decreases at almost the same speed. However, there is a large discrepancy of efficiency when the charge time exceeds about 4 h. It is clear that the charge efficiency for the PBTES filled with rock decreases faster, indicated by a steeper slop. This is due to the faster temperature rise of rock PBTES, as shown in Fig. 15, bringing increased heat loss through the wall. As a result, the charge efficiency decreases dramatically.

As shown in Figs. 15 and 16, the charge efficiency of PCM is higher than that of rock. And compared with a packed bed filled with single PCM, a packed bed filled with multiple HSMs could shorten the charge time. Meanwhile, the efficiency of multiple HSMs is close to the single PCM, which shows this filling approach have a better thermal energy storage performance.

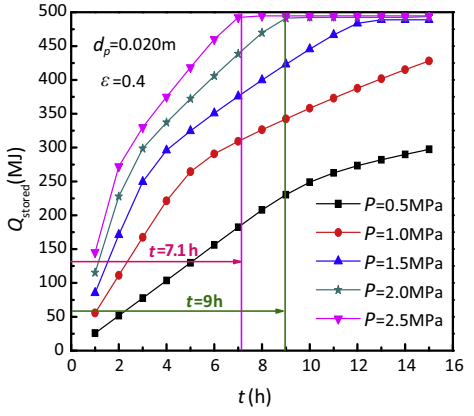

Fig. 13. Heat storage capacities versus charge time for different inlet CA pressure.

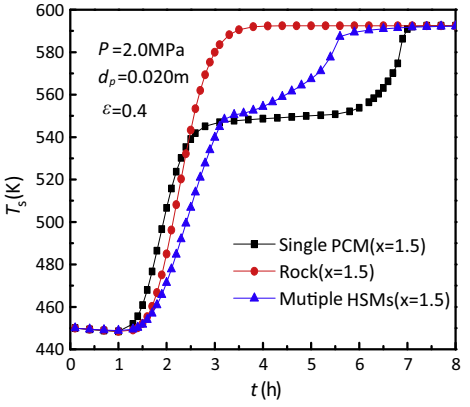

Fig. 15. Temperature profiles of solid particles versus charge time for single PCM, rock and multiple HSMs.

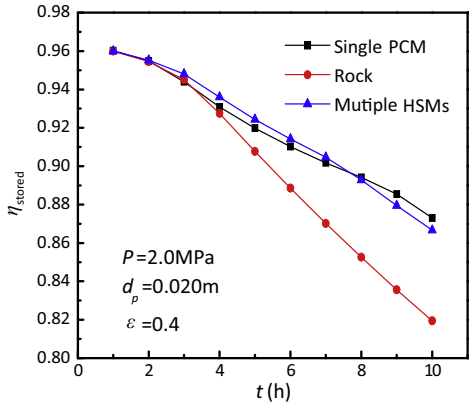

Fig. 16. Charge efficiency versus charge time for single PCM, rock and multiple HSMs.

6. Conclusion

The latent heat performance of PBTES in adiabatic CAES was analyzed numerically in the present work. In the PBTES, PCM serves as heat storage materials and store heat from CA. A mathematical model for the PBTES considering the heat transfer inside PCM and heat losses through the wall has been validated and developed.

A parametric study of the effects of porosity, particle diameter, fluid inlet pressure and filling approach on PBTES thermal behaviors were investigated for the charge process. It has been shown that higher porosity leads to markedly lower thermal storage capacity and lower charge efficiency but it takes less time to complete thermal energy storage process. With the decrease in PCM diameter, the thickness of temperature gradient decreases, resulting in higher charge efficiency. However, there is no significant discrepancy in heat storage capacity for different PCM diameters. The simulations also indicated that the inlet CA pressure had significant influence on the thermal performance of PBTES. Increasing the inlet CA pressure can shorten charge time and increase the charge efficiency. To achieve high system performance and charge efficiency, the PBTES should operate at a higher inlet CA pressure over 1.0 MPa. As compared to single rock, a packed bed filled with multiple HSMs or single PCM has better charge efficiency and shorten the charge time. This work provides a framework for interpreting the complicated thermal behavior, and optimizing the system configurations and operational strategies of the packed-bed compressed air thermal energy storage system.

Acknowledgements

The authors acknowledge the financial support provided by Natural Science Fund project in Jiangsu Province (Grant No. BK20151539), National 863 Research Program of China (Grant No. SS2013AA050801) and National Natural Science Foundation of China (No. 51176071).

References

[1] Li Y, Wang X, Li D, Ding Y. A trigeneration system based on compressed air and thermal energy storage. Appl Energy 2012;99:316–23.
[2] Marano V, Rizzo G, Tiano FA. Application of dynamic programming to the optimal management of a hybrid power plant with wind turbines, photovoltaic panels and compressed air energy storage. Appl Energy 2015;152:849–59.
[3] Bosio FD, Verda V. Thermoeconomic analysis of a Compressed Air Energy Storage (CAES) system integrated with a wind power plant in the framework of the IPEX market. Appl Energy 2012;97:173–82.
[4] Peng H, Dong HX, Ling X. Thermal investigation of PCM-based high temperature thermal energy storage in packed bed. Energy Convers Manage 2014;81:420–7.
[5] Xu C, Wang Z, He Y, Li X, Bai F. Parametric study and standby behavior of a packed-bed molten salt thermocline thermal storage system. Renew Energy 2012;48:1–9.
[6] Xu C, Wang Z, He Y, Li X, Bai F. Sensitivity analysis of the numerical study on the thermal performance of a packed-bed molten salt thermocline thermal storage system. Appl Energy 2012;92:65–75.
[7] Wu M, Xu C, He Y. Dynamic thermal performance analysis of a molten-salt packed-bed thermal energy storage system using PCM capsules. Appl Energy 2014;121:184–95.
[8] Hänchen M, Brückner S, Steinfeld A. High-temperature thermal storage using a packed bed of rocks – heat transfer analysis and experimental validation. Appl Therm Eng 2011;31:1798–806.
[9] Bouadila S, kooli Sami, Lazzaar M, Skouri S, Farhat A. Performance of a new solar air heater with packed-bed latent storage energy for nocturnal use. Appl Energy 2013;110:267–75.
[10] Yang L, Zhang X, Xu G. Thermal performance of a solar storage packed bed using spherical capsules filled with PCM having different melting points. Energy Build 2014;68:639–46.
[11] Ismail KAR, Stuginsky R. A parametric study on possible fixed bed models for PCM and sensible heat storage. Appl Therm Eng 1999;19(7):757–88.
[12] Zanganeh G, Pedretti A, Haselbacher A, et al. Design of packed bed thermal energy storage systems for high-temperature industrial process heat. Appl Energy 2015;137:812–22.
[13] Li P, Lewa JV, Karaki W. Generalized charts of energy storage effectiveness for thermocline heat storage tank design and calibration. Sol Energy 2011;85:2130–43.
[14] Zalba B, Marin JM, Cabeza LF, Mehling H. Review on thermal energy storage with phase change: materials, heat transfer analysis and applications. Appl Therm Eng 2003;23:251–83.
[15] Barton NG. Simulations of air-blown thermal storage in a rock bed. Appl Therm Eng 2013;55:43–50.
[16] Bindra H, Bueno P, Morris JF, Shinnar R. Thermal analysis and exergy evaluation of packed bed thermal storage systems. Appl Therm Eng 2013;52:255–63.
[17] Yang Z, Garimella SV. Molten-salt thermal energy storage in thermocline under different environmental boundary conditions. Appl Therm Eng 2010;87:3322–9.
[18] Aldoss TK, Rahman MM. Comparison between the single-PCM and multi-PCM thermal energy storage design. Energy Convers Manage 2014;83:79–87.
[19] Zanganeh G, Commerford M, Haselbacher A, et al. Stabilization of the outflow temperature of a packed-bed thermal energy storage by combining rocks with phase change materials. Appl Therm Eng 2014;70(1):316–20.
[20] Anderson R, Shiri S, Bindra H, Morris JF. Experimental results and modeling of energy storage and recovery in a packed bed of alumina particles. Appl Energy 2014;119:521–9.
[21] Chai L, Yang L, Liu J, Yang L, Chen H, Tan C. Performance study of a packed bed in a closed loop thermal energy storage system. Energy 2014;77:871–9.
[22] Chai L, Liu J, Wang L, Yue L, Yang L, Sheng Y, et al. Cryogenic energy storage characteristics of a packed bed at different pressures. Appl Therm Eng 2014;63:439–46.
[23] Liu J, Wang L, Yang L, Yue L, Chai L, Sheng Y, et al. Experimental study on heat storage and transfer characteristics of supercritical air in a rock bed. Int J Heat Mass Transf 2014;77:883–90.
[24] Chandra P, Willits DH. Pressure drop and heat transfer characteristics of air-rock bed thermal storage system. Sol Energy 1981;27:547–53.
[25] Coutier JP, Farber EA. Two applications of a numerical approach of heat transfer process within rock beds. Sol Energy 1982;29:451–62.
[26] Lof GOG, Hawley RW. Unsteady-state heat transfer between air and loose solids. Ind Eng Chem Res 1948;40:1061–70.
[27] Wakao N, Kagei S. Heat and mass transfer in packed beds. New York: Gordon and Breach Science Publishers; 1982.
[28] Yang J, Wang J, Bu S, Zeng M, Wang QW. Experimental analysis of forced convective heat transfer in novel structured packed beds of particles. Chem Eng Sci 2012;71:126–37.
[29] McCabe WL, Smith JC, Harriott P. Unit operations of chemical engineering. seventh ed. McGraw-Hill; 2005.
[30] Eisfeld B, Schnitzlein K. The influence of confining walls on the pressure drop in packed beds. Chem Eng Sci 2001;56(14):4321–9.
[31] Izquierdo-Barrientos MA, Sobrino C, Almendros-Ibáñez JA. Thermal energy storage in a fluidized bed of PCM. Chem Eng J 2013;230:573–83.